# Using silver nanowire antennas to enhance the conversion efficiency of photoresponsive DNA nanomotors

Quan Yuan[a], Yunfei Zhang[a], Yan Chen[a,b], Ruowen Wang[a], Chaoling Du[c], Emir Yasun[a], and Weihong Tan[a,b,1]

[a]Department of Chemistry and Department of Physiology and Functional Genomics, Shands Cancer Center and UF Genetics Institute, Center for Research at the Bio/Nano Interface, McKnight Brain Institute, University of Florida, Gainesville, FL 32611-7200; [b]State Key Laboratory of Chemo/Biosensing and Chemometrics, College of Biology, College of Chemistry and Chemical Engineering, Hunan University, Changsha 410082, China; and [c]College of Science, Nanjing University of Aeronautics and Astronautics, Nanjing 210016, China

Edited by Raoul Kopelman, University of Michigan, Ann Arbor, MI, and accepted by the Editorial Board April 13, 2011 (received for review December 7, 2010)

**Plasmonic near-field coupling can induce the enhancement of photoresponsive processes by metal nanoparticles. Advances in nanostructured metal synthesis and theoretical modeling have kept surface plasmons in the spotlight. Previous efforts have resulted in significant intensity enhancement of organic dyes and quantum dots and increased absorption efficiency of optical materials used in solar cells. Here, we report that silver nanostructures can enhance the conversion efficiency of an interesting type of photosensitive DNA nanomotor through coupling with incorporated azobenzene moieties. Spectral overlap between the azobenzene absorption band and plasmonic resonances of silver nanowires increases light absorption of photon-sensitive DNA motor molecules, leading to 85% close-open conversion efficiency. The experimental results are consistent with our theoretical calculations of the electric field distribution. This enhanced conversion of DNA nanomotors holds promise for the development of new types of molecular nanodevices for light manipulative processes and solar energy harvesting.**

energy conversion | localized surface plasmon | photo-driven nanomotor

Plants harvest solar energy by photosynthesis, in which photosensitive biomolecules absorb energy from sunlight and convert it into chemical energy. Human beings utilize solar energy by fossil fuels, solar thermal systems, and, most frequently nowadays, by photovoltaic systems based on optoelectric materials (1). The design of new synthetic materials coupled with a mechanism to capture, convert, and store photon energy will provide new ways to utilize solar energy (2, 3). However, achieving high conversion efficiency remains a challenge in such energy conversion systems.

Recently, DNA has received attention in material sciences, especially for the fabrication of nanomachines able to perform nanoscale movements in response to external stimuli (4–11). Experimental and theoretical studies on single DNA nanomachines have led to the development of new energy conversion strategies (12, 13). As one of the most popular phototransformable molecules, azobenzene and its derivatives can change the overall structure by *cis-trans* isomerisation mechanism. Using the photoisomerization of azobenzene to photo-regulate DNA hybridization, (14) we have designed a single-molecule light-driven DNA nanomotor (15) for the continuous production of energy in the form of mechanical work. This photon-fueled nanomotor is simple and easy to operate, promising a unique approach to harvest photonic energy. Herein, azobenzene derivatives act as element for energy absorption and DNA molecules movement act for mechanical energy export. As we know, solar thermal technology is a technology to harvest solar thermal energy that converts solar energy to movement of molecules and then produces heat caused by molecule thermal moving. In our design, solar energy is converted to close-open movement of DNA molecules. However, few DNA motor molecules can undergo the close-open conversion as a result of the low photoisomerization efficiency of azobenzene moieties, which is a hindrance to the further development of nanodevice applications.

Metal nanostructures act as optical antennas because the free electrons of the metallic nanostructures are in resonance with the incident light. These nonpropagating excitations of the conduction electrons of metallic nanostrucures, known as localized surface plasmon resonances, can produce an enhanced electromagnetic field localized around metal nanostructures. Plasmon coupling-induced near-field enhancement of metal nanoparticles has previously been employed to enhance fluorescence intensity of organic dyes and quantum dots and increase absorption efficiency of optical materials in solar cells. The investigation of localized surface plasmons in metal nanoparticles has received intense interest owing to a number of related unique and useful optical properties, such as confinement of light at the metal surface and the control of both the far-field and near-field distribution of light (16, 17). Depending on the details of the systems under investigation, fluorescence enhancement has been reported for fluorescent molecules, quantum dots, and rare-earth complexes near nanostructured metals through coupling with surface plasmons in metallic nanostructures (18–21). This process, referred to as metal-enhanced fluorescence, offers promise for a range of applications, including sensor technology, solid-state lighting, microarrays, and single-molecule studies. Another exciting direction for plasmonics researchers is photovoltaics. Design approaches based on plasmonics have been widely used for high-efficiency solar-cell design (22, 23). Herein, we report the use of silver nanoparticle antennas to enhance the close-open conversion efficiency of photosensitive DNA nanomotors through coupling with incorporated azobenzene moieties. The enhancement is tuned by adding silver nanoparticles with different morphologies and concentrations. Up to 85% close-open conversion efficiency can be obtained by incubating DNA molecules with silver nanowires. The conversion efficiency enhancement is a result of enhanced light absorption capabilities mainly caused by spectral overlap between azobenzene and plasmonic resonances of silver nanoparticles.

## Results and Discussion

Fig. 1 shows the design of a photo-driven DNA nanomotor. This DNA is obtained by optimizing the length and amount of azobenzene at different positions, (15) having a stable hairpin structure

Author contributions: Q.Y., Y.Z., Y.C., and W.T. designed research; Q.Y., Y.Z., Y.C., R.W., C.D., E.Y., and W.T. performed research; Q.Y., R.W., and E.Y. contributed new reagents/analytic tools; Q.Y., Y.Z., Y.C., C.D., and W.T. analyzed data; and Q.Y., Y.Z., Y.C., C.D., and W.T. wrote the paper.

The authors declare no conflict of interest.

This article is a PNAS Direct Submission. R.K. is a guest editor invited by the Editorial Board.

[1]To whom correspondence should be addressed. E-mail: tan@chem.ufl.edu.

This article contains supporting information online at www.pnas.org/lookup/suppl/doi:10.1073/pnas.1018358108/-/DCSupplemental.

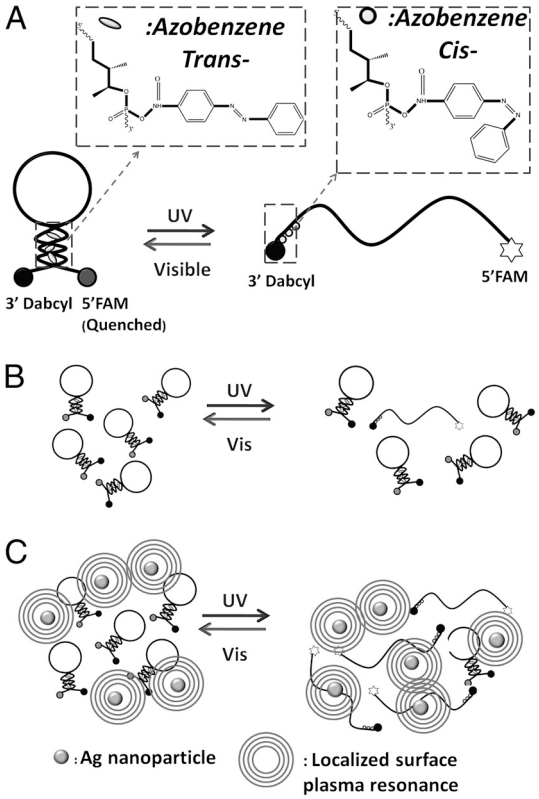


**Fig. 1.** (*A*) Structure of DNA nanomotor with three azobenzene moieties inserted in the stem duplex on the arm labeled with Dabcyl as quencher. (*B*) DNA nanomotor's behavior under UV/Visible light. (*C*) DNA nanomotor's behavior after incubation with Ag nanomaterials.

including a six-base pair stem and a nineteen-base loop. The sequence was designed as **5′FAM-CCT-AGC-TCT-AAA-TCA-CTA-TGG-TCG-CGC-TAG-G-Dabcyl3′**. A fluorophore (fluorescein isothiocyanate, FAM) and a quencher (4-dimethylaminoazobenzene-4′-carboxylic acid, Dabcyl) are labeled at both ends of the hairpin stem. Three azobenzenes are incorporated into the arm part of a hairpin loop as **5′FAM-CCT-AGC-TCT-AAA-TCA-CTA-TGG-TCG-C-Azo-GC-Azo-TA-Azo-GG-Dabcyl3′**. When the DNA motor is in the "closed" state, fluorescence is quenched through fluorescence energy transfer. Isomerization of the azobenzenes opens the loop, and the fluorophore emits. In this way, fluorescent signaling of FAM excited at 488 nm is used to monitor the photon-controlled close-open movement of the nanomotors. By setting the baseline ($I_{\mathrm{Blank}}$) to the fluorescence intensity when the azobenzene is in the *trans*- form and 100% to the fully open state after addition of excess amount of complementary DNA (cDNA 5′GGA-TCG-AGA-TTT-AGT-GAT-ACC-AGC-GCG-ATC-C3′) ($I_{\mathrm{cDNA}}$), the average close-open conversion efficiency ($\epsilon$) of the DNA nanomotor for each photon-regulation cycle can be evaluated from the equation

$$\varepsilon = \frac{I_{\mathrm{UV}} - I_{\mathrm{Blank}}}{I_{\mathrm{cDNA}} - I_{\mathrm{Blank}}} \times 100\%,$$

where $I_{\mathrm{UV}}$ is the fluorescence intensity after UV irradiation.

A layer-by-layer assembly method that was developed from that investigated for coating silica on Au nanorods, (24) was employed to construct azoDNA-nanowire hybrid nanostructures. 1 mL of Ag nanowires sample (with length of 1 μm, 2 nM) was centrifuged at 4,000 rpm for 20 min. The precipitate was redispersed in 1 mL of deionized water and then added into 100 μL of the DNA nanomotor solution (50 μM) and incubated overnight, centrifuged to remove unadsorbed DNA, and then redispersed in 1 mL of 8 mM Tris buffer. The amount of DNA adsorbed on the surface of Ag naniwires is consistent with that determined by absorption measurements, where 22% of DNA is found to be left in the supernatant after the precipitation of hybrid nanostructures by centrifugation. The isomerization experiments were performed by positioning the DNA nanomotor solution at a fixed distance from the UV lamp. As shown in Fig. 2*A*, illumination of the DNA nanomotors (no Ag present) for 5 min with 350 nm light results in only 20% loop opening. After 5 min irradiation under UV light, azoDNA-nanowire nanostructures exhibit conversion efficiency up to 85% (Fig. 2*B*). Fluorescent images were taken on a confocal laser scanning microscope. DNA nanomotor solutions, with and without Ag nanowires, were dropped onto the glass and then exposed under UV light. Fluorescence micrographs were taken every 30 s. It is obvious that the DNA nanomotor solution with Ag nanowires showed higher fluorescence intensity than that without Ag nanowires during UV illumination (Fig. 3), which is consistent with the results detected by spectrafluorometer. A more rapid increase and higher fluorescence intensity are both achieved after incubating with Ag nanowires, indicating the improved conversion efficiency of the DNA nanomotors.

The reversibility of this azoDNA nanomotor was evaluated by applying 5 min of visible irradiation and 5 min of UV irradiation for ten cycles. As shown in Fig. 4*A*, DNA nanomotors display 85% conversion efficiency with no obvious decrease after ten cycles. These results reveal that the exchange process can reversibly convert light energy directly into mechanical work. Besides the good reversibility, this nanomotor also shows high long term stability. *SI Appendix* shows the cycling of the photomediated conversion by irradiation with longer interval time. Each irradiation lasts for longer time than the former one. With increasing irradiation time, the conversion rate decreases a little. However, this azoDNA nanomotor exhibits >80% conversion efficiency even

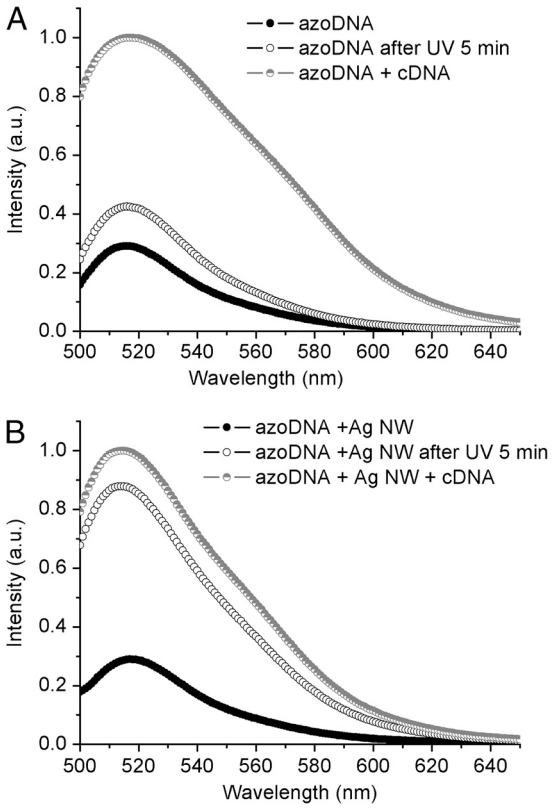


**Fig. 2.** Fluorescence spectra of (*A*) pure DNA nanomotors and (*B*) DNA nanomotors with 1 μm Ag nanowires ($\lambda_{ex}$ = 488 nm) at 25 °C. Filled circles represent pure DNA in buffer solution; open circles represent DNA with cDNA; and half-filled circles represent DNA after UV irradiation (350 nm).. Buffer: 8 mM Tris buffer pH 8.0, $Na^+$ : 8 mM, $Mg^{2+}$ : 0.8 mM, [DNA] = 5 μM, [cDNA] = 20 μM.

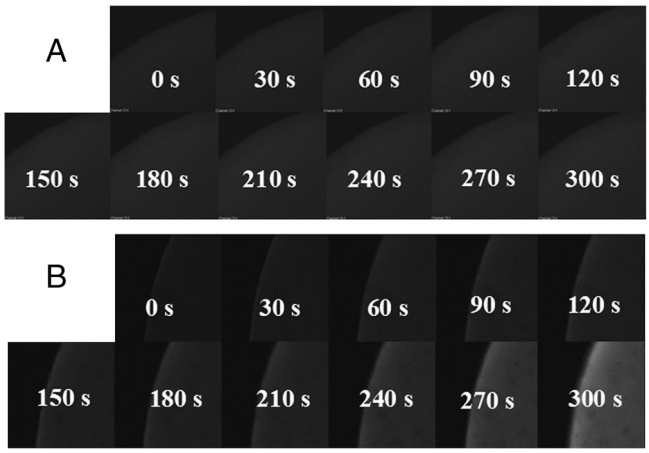


**Fig. 3.** Fluorescence micrographs of (*A*) pure DNA nanomotor solution and (*B*) DNA nanomotor solution incubated with Ag NWs under UV irradiation monitored by a laser-equipped microscope.

after 50 min irradiation. Therefore, we infer that the stability of this nanomotor will be useful in design of new nanodevices for further solar cell application. Two light sources with different wavelengths are not feasible for practical solar energy use because broad spectrum condition is not fit for controlling nanomotor open-close state. Filter switching should be applied to switch the light wavelength.

The open-close conversion efficiency was found to vary with the morphology of the Ag nanostructures. To compare the functions of different Ag nanoparticles, Ag nanospheres (Ag NSs), Ag nanoprisms (Ag NPs), and Ag nanowires (Ag NWs) with different sizes were investigated. As shown in Fig. 4*B*, Ag nanospheres and nanowires can both enhance close-open conversion efficiency, whereas Ag nanoprisms have no effect. Because the DNA molecular concentration is very high (5 μM) compared with previous reported low concentration (100 nM) (15), much more energy conversion is achieved by introducing Ag nanostructured materials, indicating their potential applications in solar cell nanodevices.

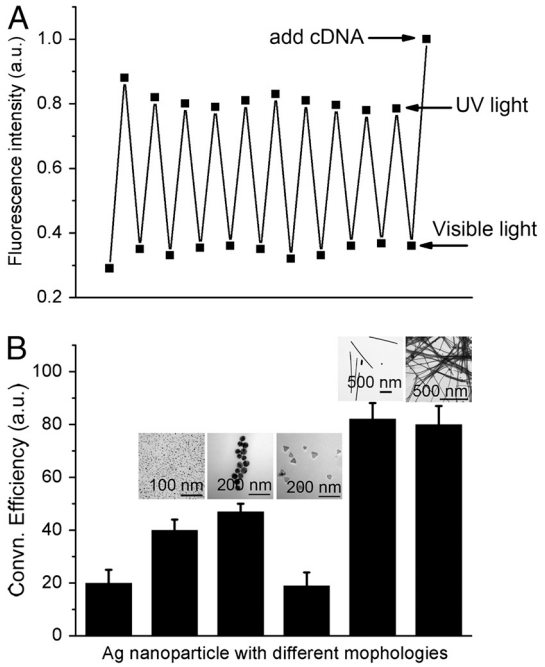


**Fig. 4.** (*A*) Cycling of close-open movement from Vis/UV irradiations at 25 °C by repeated visible and UV irradiations. UV (350 nm), 5 min; Vis (450 nm), 5 min. Fluorescence intensities were recorded immediately after each irradiation. (*B*) Conversion efficiency of DNA nanomotors with Ag nanomaterials having different morphologies. From left to right: no Ag nanoparticles, Ag NSs (6 nm diameter, 2 nM), Ag NSs (50 nm diameter, 2 nM), Ag NPs (50 nm length and 3 nm thickness, 2 nM), Ag NWs (1 μm length, 2 nM), Ag NWs (40 μm length, 2 nM).

Localized surface plasmons are nonpropagating excitations of the conduction electrons of metallic nanostructures coupled to the electromagnetic field. Ag nanoparticles in an oscillating electromagnetic field will lead to field amplification both inside and in the near-field zone outside the particles. Excited local surface plasmons have been used to elucidate the near-electric-field images of Ag nanoparticles. Although the interaction between azobenzene molecules and metal nanoparticles has been reported (25–27), for a better understanding of the physical origin of enhanced conversion efficiency, numerical simulations were performed to show near-field behavior of Ag nanoparticles using finite element method-based commercial software. The nanoparticles were simulated with the same morphology and size as those in the experiments. Fig. 5 *A*–*C* illustrate that the electric fields around the Ag nanowires, Ag nanoparticles, and Ag nanoprisms are all strongly localized. The Ag nanowires give the highest enhanced electric field distribution, as shown in Fig. 5*A*. An interesting observation from the calculated near-field distribution is that electromagnetic energy transfers into the surrounding medium, mainly at the nanowire ends, or "hot spots," which are similar to those observed in a previous report (28, 29). It is proposed that the DNA molecules are mostly attached to the two ends of the nanowire because of charging effect at the metal point (30, 31). However, compared to an Ag nanowire, a silver nanosphere shows a homogeneously enhanced electric field around it (Fig. 5*B*). The electric field around the Ag nanoprism was also calculated. A highly enhanced local electric field is present (Fig. 5*C*), showing a larger field at the angle point of the nanoprism than other positions.

To further understand the relation between optical properties of azobenzene and plasmonic properties of the Ag nanostructures, the extinction spectra of Ag nanostructures and absorption spectra of azobenzene were studied (Fig. 5*D*). The UV-visible absorption spectra of the azobenzene molecule are featured with two major absorption bands corresponding to the $S_0 \rightarrow S_1$

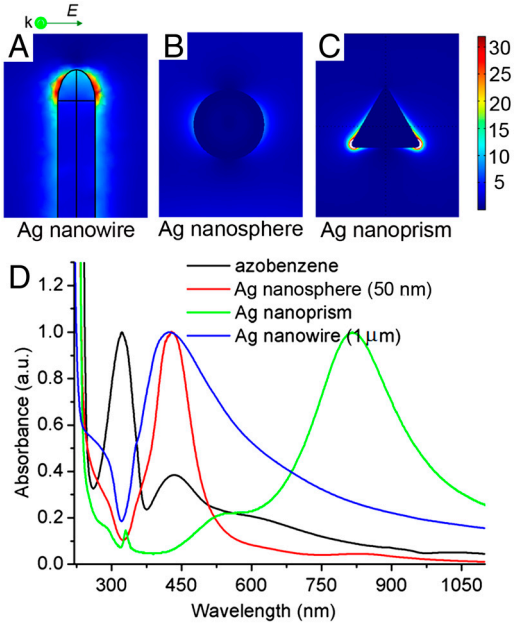


**Fig. 5.** Electric field distributions at wavelength of 350 nm ($|E|^2$) calculated for (*A*) Ag nanowire (1 μm); (*B*) Ag nanosphere (50 nm); (*C*) Ag nanoprism (50 nm). (*D*) Extinction spectra of Ag nanostructures and absorption spectra of azobenzene.

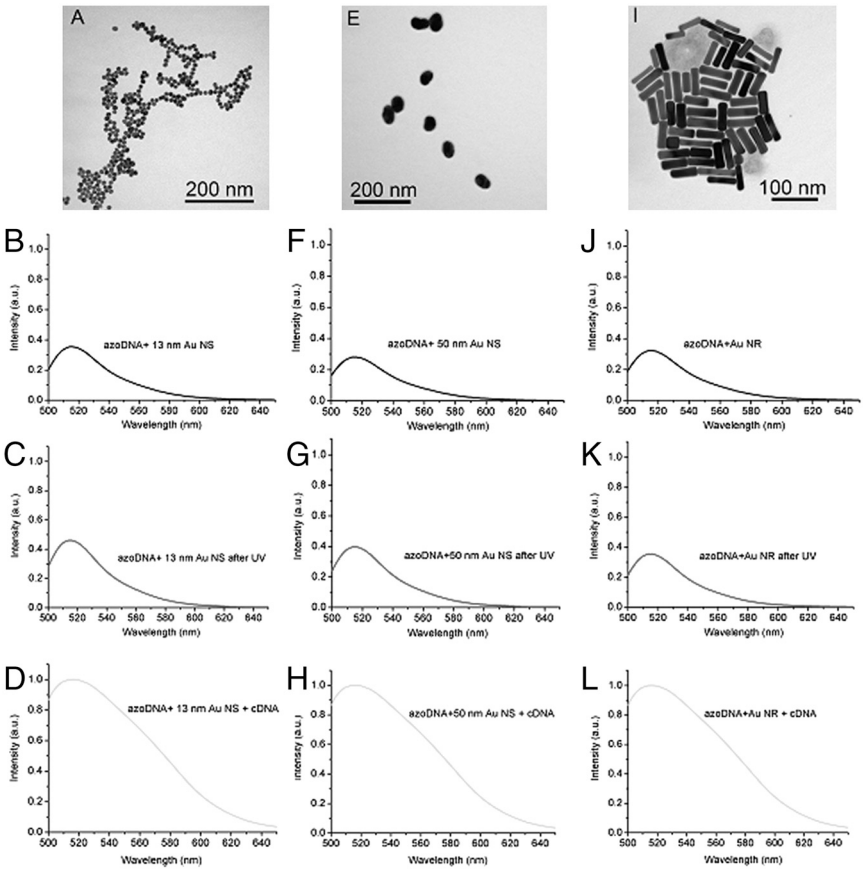


**Fig. 6.** (*A*) Au nanospheres with diameter of 13 nm. Fluorescence spectra of (*B*) DNA nanomotor incubated with Au NSs (13 nm), (*C*) DNA nanomotor incubated with Au NSs (13 nm) after 5 min UV irradiation, and (*D*) DNA nanomotor incubated with Au NSs (13 nm) after adding cDNA. (*E*) Au nanospheres with diameter of 50 nm. Fluorescence spectra of (*F*) normal DNA incubated with Au NSs (50 nm), (*G*) DNA nanomotor incubated with Au NSs (50 nm) after 5 min UV irradiation, and (*H*) DNA nanomotor incubated with Au NSs (50 nm) after adding cDNA. (*I*) Au nanorods with average length of $60 \pm 7$ nm and width of $13 \pm 3$ nm. Fluorescence spectra of (*J*) DNA nanomotor incubated with Au NRs, (*K*) normal DNA incubated with Au NRs after 5 min UV irradiation, and (*L*) DNA nanomotor incubated with Au NRs after adding cDNA. Buffer: 8 mM Tris buffer pH 8.0, $Na^+$ : 8 mM, $Mg^{2+}$ : 0.8 mM, [DNA] = 5 μM, [cDNA] = 20 μM.

and the $S_0 \rightarrow S_2$ transitions. The former transition relates to a symmetry-forbidden $n - \pi^*$ transition and exhibit a low-intensity peak at 440 nm whereas the latter transition corresponds to a symmetry-allowed $\pi - \pi^*$ transition with the much higher intensity at 320 nm (32). Silver nanospheres having a diameter of 50 nm show a narrow plasmon peak centered at 430 nm, whereas the peak of Ag nanowires (with length of 1 μm) is also around 430 nm. As shown in Fig. 5*D*, their extinction peaks overlap the absorption peak of the azobenzene molecule. Because coupling strength has been found to be strongly dependent on the spectral overlap between the molecular and plasmonic resonances (33, 34), there is, accordingly, a large coupling strength between azobenzene and the plasmonic resonance of both Ag nanospheres and nanowires. However, Ag nanoprisms give a peak located at 820 nm, which does not overlap with the absorption peak of azobenzene. As a result, there is little coupling between azobenzene and the Ag nanoprism, thus introducing very low conversion efficiency. Calculation and experimental results match very well. The combination of simulation and spectral overlap may be the main reason that Ag nanowires give the highest enhanced conversion efficiency of DNA nanomotors, whereas Ag nanoprisms cannot increase this efficiency.

Another evidence was from the photoisomerization rate increase of azobenzene molecules in the present of Ag nanowires. During the isomerization process of *trans*-azobenzene to *cis*-azobenzene, the intensity of $S_0 \rightarrow S_2$ peak at 320 nm decreases while that of $S_0 \rightarrow S_1$ transition peak at 440 nm increases (35). As illustrated in *SI Appendix*, under UV light irradiation for 210 s, the intensity of $S_0 \rightarrow S_2$ peak decreased to 75% of the original one. After adding silver nanowires, the intensity of $S_0 \rightarrow S_2$ peak decreased to 65% of the original one within 210 s (*SI Appendix*). This result indicated that more azobenzene molecules converted from *trans*- to *cis*- form in the presence of Ag nanowires. Larger percentage of azobenzene molecules absorbed the light energy due to amplified absorption cross section of azobenzene molecules by Ag nanowires (36).

Gold nanospheres and nanorods, as illustrated in Fig. 6, were also incubated with DNA nanomotors. According to fluorescence intensity detection, it was found that the conversion efficiency of DNA nanomotors was, in fact, reduced with the introduction of these nanomaterials (Fig. 6 *B–D*, *F–H*, and 6*J–L*). Moreover, the extinction peak of Au nanoparticles is around 520 nm, which is far from the position of the azobenzene absorption peak (as shown in Fig. 7 *A–C*), resulting in the absence of coupling between Au nanoparticles and DNA nanomotor molecules. Although Au nanospheres give near-field intensity similar to that of Ag nanospheres under the same incidence wavelength (Fig. 7 *D–F*), the plasmonic resonances of Au nanoparticles cannot accumulate the isomerization of azobenzene moiety.

## Conclusions

In conclusion, we have demonstrated that silver nanomaterials can enhance the rate of azobenzene isomerization in DNA nanomotors because of their local plasmon resonance-induced near-field electrodynamic environments. An open-close conversion efficiency of 85% is achieved by Ag nanowire antennas as a result of the spectral overlap between azobenzene and the plasmonic resonance of Ag nanostructures. This technique holds significant

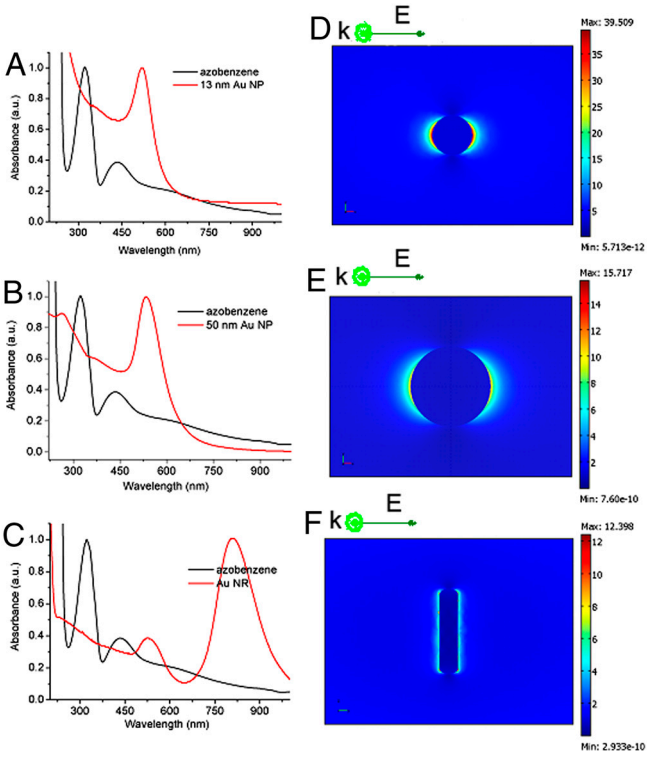


**Fig. 7.** The experimental extinction spectra of, and corresponding electric field distributions ($|E|^2$) at wavelength of 350 nm calculated for, (*A*) Au nanospheres (13 nm), (*B*) Au nanospheres (50 nm), and (*C*) Au nanorods compared with absorption spectra of azobenzene. Electric field distributions ($|E|^2$) calculated for (*D*) Au nanosphere (diameter 13 nm); (*E*) Au nanosphere (diameter 50 nm); (*F*) Au nanorod (13 nm × 60 nm).

promise for the future development of photoelectric-conversion molecular nanodevices for use in solar energy harvest.

## Materials and Methods

**Synthesis of Azobenzene Phosphoramidite.** Azobenzene phosphoramidite was synthesized according to the protocol reported by Asanuma et al. (37). **Compound 1.** $^1$H NMR ($CDCl_3$): δ 7.96-7.38 (m, 9H), δ 7.12 (d, 1H), δ 4.33 (m, 1H), δ 4.09 (m, 1H), δ 3.98 (d, 2H), δ 1.29 (d, 3H). **Compound 2.** $^1$H NMR ($CDCl_3$): δ 8.00-6.78 (m, 23H), δ 4.25 (m, 1H), δ 4.17 (m, 1H), δ 3.77 (s, 6H), δ 3.60 and 3.42 (dd, 2H), 1.23 (d, 3H). **Compound 3**. $^1$H NMR ($CDCl_3$): δ 8.00-6.79 (m, 22H), δ 6.62 (d, 1H), δ 4.48 (m, 1H), δ 4.39 (m, 1H), δ 4.21-4.10 (m, 2H), δ 3.77 (s, 6H), δ 3.57-3.34 (m, 4H), δ 2.76-2.72 (m, 2H), δ 1.30-1.25 (m, 15H). $^{31}$P ($CDCl_3$): δ 149.

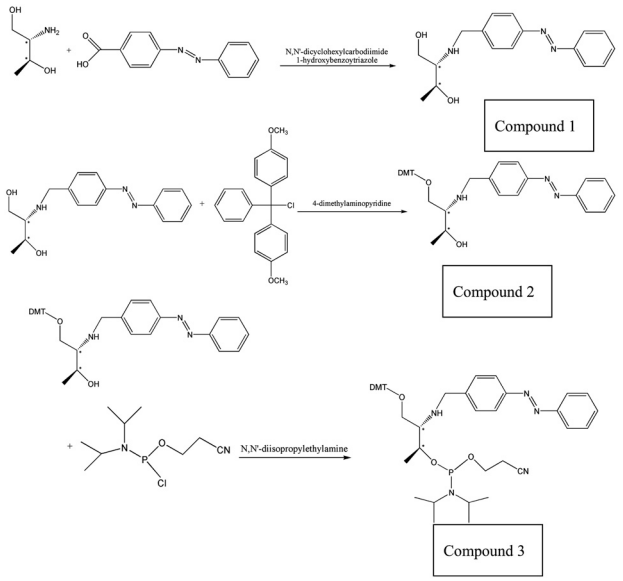


**Synthesis of DNA Nanomotors.** The designed DNA nanomotor sequence was synthesized using an ABI3400 DNA/RNA synthesizer (Applied Biosystems). The synthesis started with a 3′-Dabcyl controlled pore glass column at 1 μmole scale, and then the FAM phosphoramidite was used to couple FAM on the 5′ ends of the sequence. The azobenzene coupling was realized by using the azobenzene phosphoramidite synthesized by the protocol mentioned above. A proper amount of azobenzene phosphoramidite was dissolved in dry acetonitrile in a vial connected to the synthesizer (20 mg azobenzene phosphoramidite can make a single incorporation in the DNA at 1.0 μmole scale synthesis; generally azobenzene phosphoramidite coupling reagent can be prepared by dissolving in acetonitrile at 20 mg/200 μL). A ProStar HPLC (Varian) with a C18 column (Econosil, 5 μ, 250 mm × 4.6 mm) from Alltech was used for DNA purification. The normal DNA (5′FAM-CCT-AGC-TCT-AAA-TCA-CTA-TGG-TCG-C-AGC-ATA-AGG-Dabcyl3′) and cDNA (5′GGA-TCG-AGA-TTT-AGT-GAT-ACC-AGC-GCG-ATC-C3′) of the DNA nanomotor were synthesized by the same protocol.

**Synthesis of Ag Nanospheres.** First, 2.50 g poly(vinyl pyrrolidone) (PVP, $M_W$ = 10,000) was dissolved in 10 mL ultrapure water (Millipore, Bioscience Research Reagents); then 3 mL of $AgNO_3$ solution (188 mM) was added. Afterward, the solution was heated at 60 °C for a time certain under stirring (15 min for 6 nm Ag nanospheres and 60 min for 50 nm nanospheres), after which the product was separated by centrifugation. The nanospheres were redispersed in deionized water and the concentrations were adjusted to 2 nM.

**Synthesis of Ag Nanowires.** Ag nanowires were synthesized following a reported method (38). First, 5 mL ethylene glycol was heated to 160 °C, and then 0.5 mL 0.12 mM $PtCl_4$ solution (ethylene glycol as solvent) was injected into the solution with magnetic stirring for 4 min. Then, 2.5 mL ethylene glycol solution of $AgNO_3$ (20 mg/mL) and 5 mL ethylene glycol solution of PVP (40 mg/mL, $M_W$ = 55,000) were simultaneously injected to the ethylene glycol containing platinum seeds. This reaction mixture was stirred at 160 °C 10 min for 1 μm nanowires and 1 h for 40 μm nanowires, respectively. After cooling down to room temperature, the reaction mixture was diluted with acetone (approximate 10 times by volume) and centrifuged at 2000 rpm for 20 min. The nanowires settled down to the bottom of the container under centrifugation, whereas the nanoparticles still remaining in the liquid phase were removed using a pipette. This separation procedure was repeated several times until nanowire samples essentially free of smaller particles were obtained.

**Synthesis of Ag Nanoprisms.** A 25 mL $AgNO_3$ aqueous solution (0.1 mM) was prepared, and then 300 μL of sodium citrate (30 mM), 1.5 mL of PVP ($M_w$ = 29,000 g/mol, 3.5 mM), and 60 μL of aqueous $H_2O_2$ (30 wt%) were added under vigorous stirring at room temperature. Freshly prepared $NaBH_4$ (100 mM, 250 mL) was then rapidly injected into this mixture. The solution color changed to blue after a reaction of approximately 1 h, and Ag nanoprisms were separated by centrifugation (39).

**Synthesis of Au Nanospheres.** 0.5 mL of $HAuCl_4$ (0.01 M) solution was added to 20 mL of ultrapure water and heated to boiling under vigorous stirring. Then, freshly prepared sodium citrate solution (0.034 M, 0.40 mL for the 13 nm Au nanospheres and 0.5–0.175 mL for the 50 nm Au nanospheres) was added. The solution was kept boiling until the color turned from dark blue to red. Stirring was maintained until the solution cooled down to room temperature, and then the products were obtained by centrifugation.

**Synthesis of Au Nanorods.** Cetyltrimethylammonium bromide (CTAB) aqueous solution (0.2 M, 5 mL) was mixed with $NaAuCl_4$ (0.5 mM, 5 mL). Freshly prepared, ice-cold 0.01 M $NaBH_4$ (0.6 mL) was added to this solution all at once, followed by rapid inversion mixing for 2 min. The resulting CTAB-stabilized gold nanoparticle seed solution was kept at room temperature for 2 hrs. For seed-mediated growth, $NaAuCl_4$ (1 mM, 50 mL) and $AgNO_3$ (0.1 M, 0.1 mL) were added to CTAB (50 mL, 0.2 M). After gentle mixing of the solution, freshly prepared ascorbic acid solution (78.8 mM, 0.7 mL) was added as a mild reducing agent. The reaction mixture was mixed by gentle inversion for 10 s. Then a portion of the seed solution (50 mL) was mixed with glycine solution (0.2 M, 50 mL) and left undisturbed at least overnight to form Au nanorods.

**Light Sources.** To test the efficiency of azobenzene isomerization and the opening/closing of the hairpin structure under specific irradiation, two kinds of light sources were used. A 23 W 60 Hz UV lamp with the wavelength at 350 nm was used to convert the azobenzene DNA motor from *trans*- to

*cis*-, which opened the DNA hairpin structure, and a 60 W table lamp with a 450 nm filter was used to convert the azobenzene DNA motor from *cis*- to *trans*-, which closed the DNA hairpin structure.

**Calculation Method.** We have performed numerical simulations of the field ($|E|^2$) intensity distributions around the different nanostructures by finite element method using the commercial software of COMSOL Femlab. Here, the 3D radio frequency model of the software was used. The incident light wavelength was chosen to be 350 nm according to our experiment whereas the optical constant of the silver and gold is referred to the data reported by Johnson et al. (40). To avoid spurious reflection effects at the simulation zone boundaries, perfectly matched layers have been adopted.

**Instruments.** Transmission electron microscopy (TEM) images were obtained on a Hitachi H-7000 transmission electron microscope under a working voltage of 100 kV. Absorbance was measured on a Cary Bio-300 UV spectrometer (Varian). Fluorescence measurements were performed on a Fluorolog-Tau-3 spectrofluorometer (Jobin Yvon). The fluorescence images were taken by CLSM (IX81, Olympus).

**ACKNOWLEDGMENTS.** We acknowledge the Interdisciplinary Center for Biotechnology Research (ICBR) at the University of Florida for TEM technical support. This work is supported by grants awarded by the National Institutes of Health (GM066137, GM079359) and by the National Key Scientific Program of China (2011CB911000) and China National Grand Program (2009ZX10004-312).

1. US Department of Energy (2005) *Office of Science Basic Research Needs for Solar Energy Utilization*, Available at http://www.sc.doe.gov/bes/reports/files/SEU_rpt.pdf.
2. Balzani V, Venturi M, Credi A (2004) *Molecular Devices and Machines: A Journey into the Nanoworld* (Wiley, Weinheim).
3. Masiero S, Lena S, Pieraccini S, Spada GP (2008) The direct conversion of light into continuous mechanical energy by photoreversible self-assembly: A prototype of a light-powered engine. *Angew Chem Int Ed* 47:3184–3187.
4. Mao C, Sun W, Shen Z, Seeman NC (1999) A nanomechanical device based on the B-Z transition of DNA. *Nature* 397:144–146.
5. Yurke B, Turberfield AJ, Mills AP, Simmel FC, Neumann JL (2000) A DNA-fuelled molecular machine made of DNA. *Nature* 406:605–608.
6. Yan H, Zhang X, Shen Z, Seeman NC (2002) A robust DNA mechanical device controlled by hybridization topology. *Nature* 415:62–65.
7. Li JW, Tan WH (2002) A single DNA molecule nanomotor. *Nano Lett* 2:315–318.
8. Liu D, Balasubramanian S (2003) A proton-fuelled DNA nanomachine. *Angew Chem Int Ed* 42:5734–5736.
9. Shin JS, Pierce NA (2004) A synthetic DNA walker for molecular transport. *J Chem Soc* 126:10834–10835.
10. Bath J, Turberfield AJ (2007) DNA nanomachines. *Nat Nanotechnol* 2:275–284.
11. Modi S, et al. (2009) A DNA nanomachine that maps spatial and temporal pH changes inside living cells. *Nat Nanotechnol* 4:325–330.
12. Turberfield AJ, et al. (2003) DNA fuel for free-running nanomachines. *Phys Rev Lett* 90:118102-1–118102-4.
13. Chen Y, Wang M, Mao C (2004) An autonomous DNA nanomotor powered by a DNA enzyme. *Angew Chem Int Ed* 43:3554–3557.
14. Dohno C, Uno S, Nakatani K (2007) Photoswitchable molecular glue for DNA. *J Am Chem Soc* 129:11898–11899.
15. Kang HZ, et al. (2009) Single-DNA Molecule nanomotor regulated by photons. *Nano Lett* 9:2690–2696.
16. Barnes WL, Dereux A, Ebbesen TW (2003) Surface plasmon subwavelength optics. *Nature* 424:824–830.
17. Lal S, Link S, Halas NJ (2007) Plasmonics: From surface plasmon sensing to plasmon waveguiding. *Nat Photonics* 1:641–648.
18. Liu N, Prall BS, Klimov V (2006) Hybrid gold/silica/nanocrystal-quantum-dot superstructures: synthesis and analysis of semiconductor—metal interactions. *J Am Chem Soc* 128:15362–15363.
19. Pompa PP, et al. (2006) Metal-enhanced fluorescence of colloidal nanocrystals with nanoscale control. *Nat Nanotechnol* 1:126–130.
20. Bek A, et al. (2008) Fluorescence enhancement in hot spots of AFM-designed gold nanoparticle sandwiches. *Nano Lett* 8:485–490.
21. Zhang H, et al. (2010) Plasmonic modulation of the upconversion fluorescence in $NaYF_4$:Yb/Tm hexaplate nanocrystals using gold nanoparticles or nanoshells. *Angew Chem Int Ed* 49:2865–2868.
22. Polman A (2008) Plasmonics applied. *Science* 322:868–869.
23. Atwater HA, Polman A (2010) Plasmonics for improved photovoltaic devices. *Nat Mater* 9:205–213.
24. Pastoriza-Santos I, Pérez-Juste J, Liz-Marzán LM (2006) Silica-coating and hydrophobation of CTAB-stabilized gold nanorods. *Chem Mater* 18:2465–2467.
25. Ahonen P, Schiffrin DJ, Paprotny J, Kontturi K (2007) Optical switching of coupled plasmons of Ag-nanoparticles by photoisomerisation of an azobenzene ligand. *Phys Chem Chem Phys* 9:651–658.
26. Manna A, et al. (2003) Optimized photoisomerization on gold nanoparticles capped by unsymmetrical azobenzene disulfides. *Chem Mater* 15:20–28.
27. Evans SD, et al. (2008) Photoswitching of azobenzene derivatives formed on planar and colloidal gold surfaces. *Langmuir* 14:6436–6440.
28. Du CL, You YM, Zhang XJ, Johnson K, Shen ZX (2009) Polarization-dependent confocal imaging of individual Ag nanorods and nanoparticles. *Plasmonics* 4:217–222.
29. Wei H, Reyes-Coronado A, Nordlander P, Aizpurua J, Xu HX (2010) Multipolar plasmon resonances in individual Ag nanorice. *ACS Nano* 4:2649–2654.
30. Caswell KK, Wilson JN, Bunz UHF, Murphy CJ (2003) Preferential end-to-end assembly of gold nanorods by biotin—streptavidin connectors. *J Am Chem Soc* 125:13914–13915.
31. Sudeep PK, Joseph STS, Thomas KG (2005) Selective detection of cysteine and glutathione using gold nanorods. *J Am Chem Soc* 127:6516–6517.
32. Zimmerman G, Chow LY, Paik UJ (1958) The photochemical isomerization of azobenzene. *J Am Chem Soc* 80:3528–3531.
33. Ni WH, Yang Z, Chen HJ, Li L, Wang JF (2008) Coupling between molecular and plasmonic resonances in freestanding dye-gold nanorod hybrid nanostructures. *J Am Chem Soc* 130:6692–6693.
34. Witlicki ED, et al. (2010) Turning on resonant SERRS using the chromophore—plasmon coupling created by host—guest complexation at a plasmonic nanoarray. *J Am Chem Soc* 132:6099–6107.
35. Kumard GS, Neckers C (1989) Photochemistry of azobenzene-containing polymers. *Chem Rev* 89:1915–1925.
36. Ambjörnsson T, Mukhopadhyay G, Apell SP, Käll M (2006) Resonant coupling between localized plasmons and anisotropic molecular coatings in ellipsoidal metal nanoparticles. *Phys Rev B* 73:085412-1–085412-10.
37. Asanuma H, et al. (2007) Synthesis of azobenzene-tethered DNA for reversible photoregulation of DNA functions: hybridization and transcription. *Nat Protoc* 2:203–212.
38. Sun YG, Gates B, Mayers B, Xia YN (2002) Crystalline silver nanowires by soft solution processing. *Nano Lett* 2:165–168.
39. Zhang Q, et al. (2009) Reconstruction of Ag nanoplates by UV irradiation: tailored optical property and enhanced stability. *Angew Chem Int Ed* 48:3516–3519.
40. Johnson PB, Christy RW (1972) Optical constants of noble metals. *Phys Rev B* 6:4370–4739.